University of Baghdad
College of Engineering
JE
JOURNAL OF ENGINEERING

Journal of Engineering
journal homepage: www.joe.uobaghdad.edu.iq
Number 5 Volume 25 May 2019

Mechanical and Energy Engineering

Non-Destructive Damage Assessment of Five Layers Fiber Glass / Polyester Composite Materials Laminated Plate by Using Lamb Waves Simulation

Hani Kamal Chyad Khalil*
College of Engineering–University of Baghdad

Dr. Nabil Hassan Hadi
College of Engineering–University of Baghdad

ABSTRACT

Composite materials are widely used in the engineered assets as aerospace structures, marine and air navigation owing to their high strength/weight ratios. Detection and identification of damage in the composite structures are considered as an important part of monitoring and repairing of structural systems during the service to avoid instantaneous failure. Effective cost and reliability are essential during the process of detecting. The Lamb wave method is an effective and sensitive technique to tiny damage and can be applied for structural health monitoring using low energy sensors; it can provide good information about the condition of the structure during its operation by analyzing the propagation of the wave in the plate. This paper presented the results and conclusions of a theoretical, numerical and experimental study of this method which was used for damage detection in the five layers fiberglass/polyester composite laminated plate, the fiber layer type is plain woven ($0^o/90^o$). The numerical analysis has been carried out by FEM using ABAQUS software for intact and cracked test specimen with the various boundary conditions and excitation frequencies, the results obtained have been confirmed experimentally by using piezoelectric wafer transducers (PZT) as actuator and sensor for both cases of experiments, it has been noted as a good agreement between experimental and numerical results.

Keywords: composite laminated plate, Lamb wave, piezoelectric wafer transducers, damage.

تقييم الضرر غير ألاتلافي لصفيحة المواد المركبة المصنعة من الياف الزجاج / البوليستر خماسية الطبقات بإستخدام محاكاة موجات لامب

هاني كمال جياد خليل
كلية الهندسة - جامعة بغداد

د. نبيل حسن هادي
كلية الهندسة - جامعة بغداد

الخلاصة

تستخدم المواد المركبة على نطاق واسع في الأصول الهندسية كهياكل الفضاء والملاحة البحرية والجوية بسبب نسب القوة/الوزن العالية. يعتبر الكشف عن الأضرار في الهياكل المركبة وتحديدها جزءًا هامًا من مراقبة الأنظمة الهيكلية وإصلاحها أثناء الخدمة لتجنب الفشل الفوري. تعتبر التكلفة الفعالة والموثوقية ضرورية أثناء عملية الكشف. طريقة موجة لامب هي تقنية فعالة وحساسة للأضرار الصغيرة ويمكن تطبيقها لمراقبة السلامة الهيكلية باستخدام أجهزة استشعار منخفضة الطاقة. حيث يمكن أن توفر معلومات جيدة حول حالة الهيكل أثناء تشغيله من خلال تحليل انتشار الموجة في الصفيحة. عرض هذه البحث نتائج واستنتاجات الدراسة النظرية والعددية والتجريبية لهذه الطريقة التي تم استخدامها للكشف عن الأضرار لصفيحة المواد المركبة المصنعة من الياف الزجاج / البوليستر خماسية الطبقات، نوع طبقة الألياف هو نسج عادي ($0^o/90^o$). تم إجراء التحليل العددي بواسطة FEM باستخدام برنامج ABAQUS لعينات اختبار سليمة ومتصدعة مع مختلف شروط الحدود وترددات الإثارة ،

*Corresponding author
Peer review under the responsibility of University of Baghdad.
https://doi.org/10.31026/j.eng.2019.05.02

Article received: 14/5/2018
Article accepted: 21/6/2018

النتائج التي تم الحصول عليها تم تأكيدها تجريبيا باستخدام محولات الرقاقة كهرضغطية (PZT) كمشغل ومستشعر لكلتا الحالتين من التجارب، وقد لوحظ اتفاق جيد بين النتائج التجريبية والعددية.
الكلمات الرئيسية : صفيحة محددة مركبة، موجة لامب، محولات طاقة كهروضغطية رقائقية، ضرر .

1. INTRODUCTION

Failure of fiber-reinforced composite materials takes several forms; fibers breakage, fibers buckling, delamination and matrix yielding or cracking. Local Failure or micro-failure reduces the stiffness and strength of the composite. Micro-failure does not necessarily lead to sudden collapse because the surrounding matrix supports the fibers; the growth of failure during the operating time is serious in composite structures. Lamb waves at ultrasonic frequencies have the ability to propagate for a long distance in thin elastic plates with little attenuation and have high sensitivity to damage; it can be activated to propagate across the structure to demonstrate their use in *pitch-catch* behavior to monitor plate integrity. Guided waves (Lamb waves) can be used for non-destructive testing of aluminum aircraft panels, composite laminated plate and another plate-like object. The difficulty in applying Lamb waves includes the continuation of multiple modes and each of them highly dispersive, **Graff, 1975** and **Rose, 2014**, which can make the interpretation of pulse-echo response difficult or impossible. In this paper, it was shown that the selective generation of the S_0 wave conquered this difficulty; therefore, selection of pulse characteristics to achieve selective generation should be considered obligatory for this application. The modern use of single piezoelectric wafer transducers, surface-mounted on the plate, has attracted great interest, **Kessler, et al., 2003** and **Giurgiutiu,** and **Zagrai, 2000**. Simplicity inherent in piezoelectric type wafer transformers is heartening for practical reasons and its low cost. **Giurgiutiu, 2002**, published a theoretical explanation for the mode selectivity of a PZT wafer transducer, with accompanying experiments, the results were good and important. **Nieuwenhuis, et al., 2004**, presented a study about using of finite element simulation and experiments to more explore the operation of the wafer transducer and Lamb wave generation for structural health monitoring. The wave velocities and the received voltage signals due to A_0 and S_0 modes at an output transducer as a function of pulse center frequency have been calculated. The results demonstrate that a piezoelectric wafer transducer can be used for selective excitation of the S_0 mode. In this research, Lamb wave technique was used with a pitch-catch configuration to detect plate damage numerically and experimentally, with smart sensor and actuator type piezoelectric lead zirconate titanate (PZT) wafer transducer, with different boundary conditions.

2. LAMB WAVE THEORY

The theoretical part of Lamb wave propagation started with a summary of the beginning of the 2D equations in a flat plate, which has been followed by the method of Viktorov (1967). Lamb wave dispersion equations have been started from the wave equations in elastic isotropic medium **Wilcox**, **1998**.

2.1 Propagation of Wave in Isotropic Elastic Medium

A Cartesian axes system in the *x*, *y*, and *z*-directions was defined in the materials being studied to discover the wave equation. When ρ is the density of material and with considering the equilibrium cube element of material and by using Hooke's law to link the relationship between stresses and strains, the differential equation for the displacement field has been deduced, **Rose, 2014** as:

$$\begin{aligned}
\rho\frac{\partial^2 u}{\partial_{t^2}} &= (\lambda+\mu)\frac{\partial}{\partial x}\left(\frac{\partial u}{\partial x}+\frac{\partial v}{\partial y}+\frac{\partial w}{\partial z}\right)+\mu\left(\frac{\partial^2}{\partial x^2}+\frac{\partial^2}{\partial y^2}+\frac{\partial^2}{\partial z^2}\right)u+f_x\\
\rho\frac{\partial^2 v}{\partial_{t^2}} &= (\lambda+\mu)\frac{\partial}{\partial y}\left(\frac{\partial u}{\partial x}+\frac{\partial v}{\partial y}+\frac{\partial w}{\partial z}\right)+\mu\left(\frac{\partial^2}{\partial x^2}+\frac{\partial^2}{\partial y^2}+\frac{\partial^2}{\partial z^2}\right)v+f_y\\
\rho\frac{\partial^2 w}{\partial_{t^2}} &= (\lambda+\mu)\frac{\partial}{\partial z}\left(\frac{\partial u}{\partial x}+\frac{\partial v}{\partial y}+\frac{\partial w}{\partial z}\right)+\mu\left(\frac{\partial^2}{\partial x^2}+\frac{\partial^2}{\partial y^2}+\frac{\partial^2}{\partial z^2}\right)w+f_z
\end{aligned} \quad (1)$$

Where *u*, *v* and *w* are the displacements in the *x*, *y*, and *z*-direction, λ and μ were the Lamé constants of the material, *f* was the centrifugal force and *t* represented the time. This was the motion differential equations *(Navier's-Lamés displacement equations*) which referred to as the wave equations. In this research, the centrifugal force was considered zero *f* = 0, **Lammering, et al., 2017**.

$$\lambda = \frac{\upsilon E}{(1+\upsilon)(1-2\upsilon)} = \frac{2\mu.\upsilon}{1-2\upsilon} \quad , \ \mu = \frac{E}{2(1+\upsilon)} \tag{2}$$

The solution of the wave equations has been considered here with waves propagating in a continuous homogeneous plane at *x*-direction. In those waves, every wave-front was an infinitely plane parallel with the *y z* plane, and the displacement field was independent of the *y* and *z*-direction. For this reason, a harmonic spatial reliance was described by *exp(ikx)*, where *k* indicated to the wave-number and $i = \sqrt{-1}$. The solution can be in two forms, depending on the movement of the particles, parallel or vertical on the occurrence of the wave propagation, *longitudinal* and *transverse* waves**,** respectively, as shown in **Fig.1**.

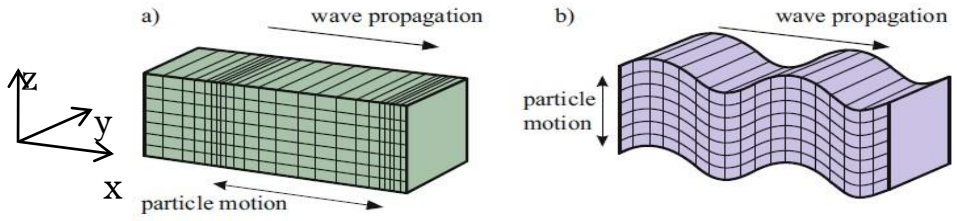

Figure 1. (a)-Longitudinal wave. (b)-Transversal wave, **Lammering, et al., 2017**.

The displacement field in the longitudinal wave is then given by:

$$\begin{aligned} u &= A_x exp(kx - i\omega t) \\ v &= 0 \\ w &= 0 \end{aligned} \tag{3}$$

Where A_x is constant, ω is angular frequency.

Substitution the Eq. (3) into Eq. (1), the result is:

$$\frac{\omega}{k} = \sqrt{\frac{\lambda+2\mu}{\rho}} = c_l \tag{4}$$

Where c_l is the longitudinal velocity (*phase velocity*) it is wave crests propagate, in this case, the particle motion has been constrained in the direction of wave propagation.

The displacement field in the transverse wave is then given by:

$$\begin{aligned} u &= 0 \\ v &= A_y exp(kx - i\omega t) \\ w &= A_z exp(kx - i\omega t) \end{aligned} \tag{5}$$

Where, A_y and A_z are constants, unlike the displacement field for longitudinal waves.

Substitution the Eq. (5) into Eq. (1) result gives:

$$\frac{\omega}{k} = \sqrt{\frac{\mu}{\rho}} = c_t \quad (6)$$

Where c_t the phase velocity of the propagating transverse wave, it referred to shear wave velocity because of the particle motion is at right angles to the direction of propagation.

Eq. (1) can be rewritten in potential function form to decompose the displacement field $\vec{u}$ into two fields, associated with a longitudinal and transverse wave which is non-rotational and non-divergent, respectively. If the displacement field was the *grad* of scalar field$\emptyset$, the vector showed the displacements field is non-rotational. And, if the displacement field was the *curl* vector field $\vec{\psi}$, the displacement field shown to be non-divergent. Then, the displacement field for any particle can be written, **Wilcox**, **1998**, as:

$$\vec{u} = \nabla\emptyset + \nabla \times \vec{\psi} \quad (7)$$

Where $\nabla = (\frac{\partial}{\partial x} + \frac{\partial}{\partial y} + \frac{\partial}{\partial z})$

$\emptyset$ and $\vec{\psi}$ are the potential functions. Then, can be rewriting the wave equation in term of the potential function as:

$$\rho \frac{\partial^2 \emptyset}{\partial_{t^2}} = (\lambda + 2\mu)\nabla^2\emptyset \quad \text{For longitudinal waves} \quad (8)$$

$$\rho \frac{\partial^2 \vec{\psi}}{\partial_{t^2}} = \mu\nabla^2\vec{\psi} \quad \text{For transverse waves} \quad (9)$$

2.2 Wave Propagation in Flat Plate

The plate with the Cartesian axis was defined as the *(x, y)* axes in the plane of the plate and the *z*-axis perpendicular to the plane of it. The plate was extending to infinitely in the *x* and *y* directions, the *z*-axis was located in midway through the plate thickness (h) as shown in **Fig. 2**. Hence, the boundary conditions which wave in the plate must satisfy has been given by:

$$\begin{aligned} \sigma_{zz|_{z=\pm h/2}} &= 0 \\ \tau_{xz|_{z=\pm h/2}} &= 0 \\ \tau_{yz|_{z=\pm h/2}} &= 0 \end{aligned} \quad (10)$$

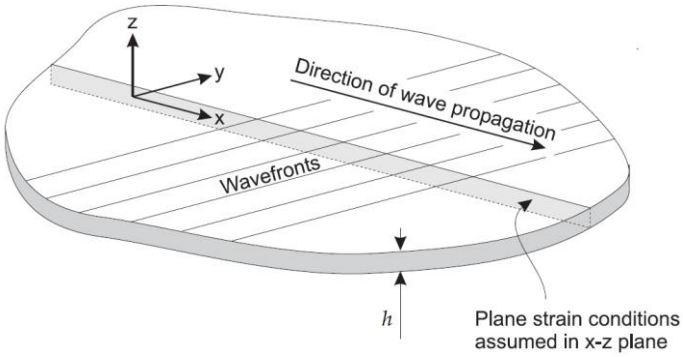

Figure 2. Diagram of the flat isotropic plate, showing the orientation of axes, wave propagation direction and wavefronts, **Wilcox**, **1998.**

Lamb wave propagates in the *x*-direction only, this assumption has been considered. This means the wave-fronts are assumed to be infinitely in the *y*-direction as illustrated in schematic **Fig. 2**

that means the behaviors of the waves are not dependent on the *y*-direction, hence $\frac{\partial}{\partial y} = 0$. The second condition, does not exist displacement in the *y* direction, hence the solution set include only actual Lamb wave and does not contain transverse wave (SH) that rotation about *z* axis, so *v=0*. Then there was rotation about axes in the *y* direction only, therefore the $\vec{\psi}$ include components in the *y* direction (ψ_y) only. The wave equations, Eq. (8) and (9), will be as **Wilcox**, **1998**:

$$\rho \frac{\partial^2 \emptyset}{\partial_{t^2}} = (\lambda + 2\mu)\left(\frac{\partial^2 \emptyset}{\partial x^2} + \frac{\partial^2 \emptyset}{\partial z^2}\right) \quad (11)$$

$$\rho \frac{\partial^2 \psi_y}{\partial_{t^2}} = \mu\left(\frac{\partial^2 \psi_y}{\partial x^2} + \frac{\partial^2 \psi_y}{\partial z^2}\right) \quad (12)$$

Defining longitudinal and transverse wavenumbers, k_l and k_t respectively, as follows:

$$k_l = \omega\sqrt{\frac{\rho}{\lambda+2\mu}} = \frac{\omega}{c_l} \quad (13)$$

$$k_t = \omega\sqrt{\frac{\rho}{\mu}} = \frac{\omega}{c_t} \quad (14)$$

Assuming a temporal harmonic dependence of *exp(iωt)* enables the wave equations to be further reduced to:

$$\frac{\partial^2 \emptyset}{\partial x^2} + \frac{\partial^2 \emptyset}{\partial z^2} + k_l^2 \emptyset = 0 \quad (15)$$

$$\frac{\partial^2 \psi_y}{\partial x^2} + \frac{\partial^2 \psi_y}{\partial z^2} + k_t^2 \psi_y = 0 \quad (16)$$

2.3 Solution with Symmetric and Anti -Symmetric Mode

The calculation is concerned with waves propagating along the plate, hence a new wavenumber (*k*) has been introduced in this direction. When the waves crests are straight, a spatial harmonic solution of the potentials functions governed by *exp(ikx)* was assumed (this was the difference between the solution for straight crests Lamb waves and that for circular crests Lamb waves), **Wilcox**, **1998**. The potential functions satisfy to reduce wave equations, Eq. (15) and (16) as:

$$\emptyset = (A_1 \sin q_l z + A_2 \cos q_l z)e^{i(kx-\omega t)} \quad (17)$$
$$\psi_y = (B_1 \sin q_t z + B_2 \cos q_t z)e^{i(kx-\omega t)} \quad (18)$$

Where A_1, A_2, B_1, and B_2 are four constants determined by the boundary conditions,

$q_l = \sqrt{{k_l}^2 - k^2}$, $q_t = \sqrt{{k_t}^2 - k^2}$ and $k = \frac{2\pi}{\lambda_{wave}}$

There with the in-plane (*u*) and out-of-plane displacements (*w*) become:

$$u = \{ik[A_1 \sin(q_l z) + A_2 \cos(q_l z)] - [q_t B_1 \cos(q_t z) - q_t B_2 \sin(q_t z)]\}e^{i(kx-\omega t)} \quad (19)$$
$$w = \{[q_l A_1 \cos(q_l z) - q_l A_2 \sin(q_l z)] + ik[B_1 \sin(q_t z) + B_2 \cos(q_t z)]\}e^{i(kx-\omega t)} \quad (20)$$

In Eq. (19) and Eq. (20) the field quantities contained sine and cosine terms with amount *z*, which are odd and even functions in *z*, respectively. So, the displacements *u* and *w* are divided into the

symmetric and anti-symmetric part. If *u* comprises cosine terms, then the displacements motion during *x*-direction is symmetric concerning the mid-plane of the plate. So, the displacements motion of in-plane was anti-symmetric for sin terms of *u*. The same applies to *the z*-direction. Based on the field of displacement u of wave propagation, can differentiate between a symmetrical and an anti-symmetrical mode, as shown in **Fig. 3**.

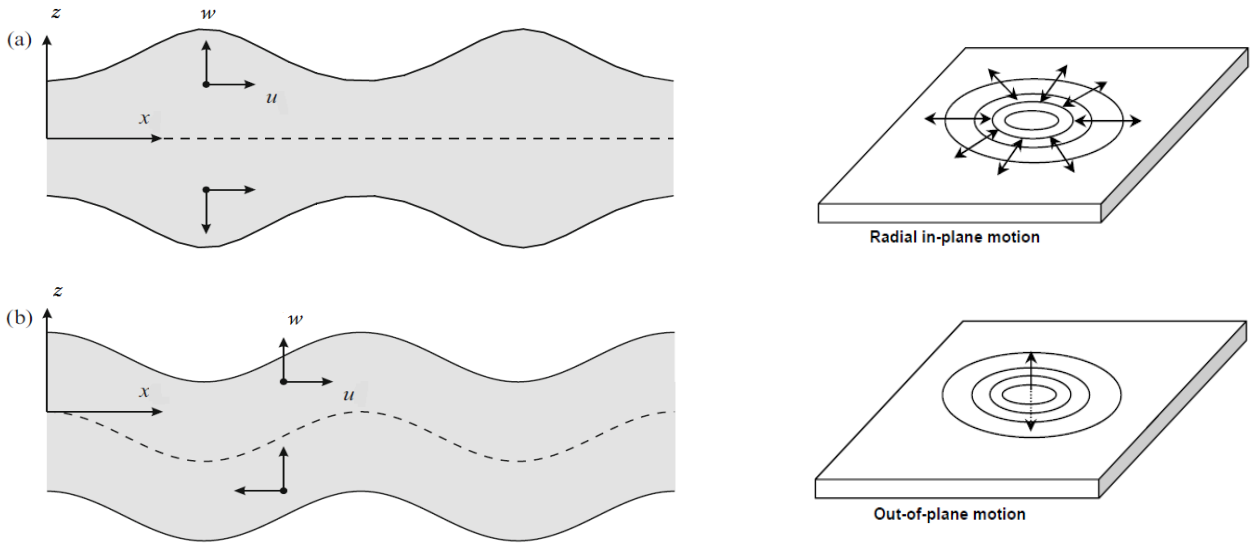

Figure 3. Displacement components of the fundamental Lamb wave modes.
(a) Symmetric wave (S_0). (b) Anti-symmetric wave (A_0), **Lammering, et al., 2017**.

Symmetric mode:

$$u(x,+z) = u(x,-z)$$
$$w(x,+z) = -w(x,-z) \quad (21)$$

Anti-symmetric mode:

$$u(x,+z) = -u(x,-z)$$
$$w(x,+z) = w(x,-z) \quad (22)$$

For the symmetric mode, one obtains:

$$u^{sym} = [ikA_2\cos(q_l z) - q_t B_1 \cos(q_t z)]e^{i(kx-\omega t)}$$
$$w^{sym} = [-q_l A_2 \sin(q_l z) + ikB_1 \sin(q_t z)]e^{i(kx-\omega t)} \quad (23)$$

And the anti-symmetric waves are given as:

$$u^{anti} = [ikA_1 \sin(q_l z) + q_t B_2 \sin(q_t z)]e^{i(kx-\omega t)}$$
$$w^{anti} = [q_l A_1 \cos(q_l z) + ikB_2 \cos(q_t z)]e^{i(kx-\omega t)} \quad (24)$$

To determine the constants *Ai* and *Bi* (for $i = 1, 2$) as well as the angular wavenumber *k* in Eq. (23) and Eq. (24) the stress boundary conditions are included at the surfaces of the infinitely extended plate. And as explained previously from the displacement field, the strain field may be calculated and finally, Hooke's law, **Howatson, et al., 1972**, is used to obtain the relevant components of the stress field, **Lammering, et al., 2017**.
Stress equations of the symmetric waves:

$$\tau_{zx}^{sym} = \mu[-2ikq_l A_2 \sin(q_l z) + (q_t^2 - k^2)B_1 \sin(q_t z)]e^{i(kx-\omega t)}$$
$$\sigma_{zz}^{sym} = \mu[-(q_t^2 - k^2)A_2 \cos(q_l z) + 2ikq_t B_1 \cos(q_t z)]e^{i(kx-\omega t)} \quad (25)$$

And the anti-symmetric ones:

$$\tau_{zx}^{anti} = \mu[2ikq_l A_1 \cos(q_l z) + (q_t^2 - k^2)B_2 \cos(q_t z)]e^{i(kx-\omega t)}$$
$$\sigma_{zz}^{anti} = \mu[-(q_t^2 - k^2)A_1 \sin(q_l z) - 2ikq_t B_2 \sin(q_t z)]e^{i(kx-\omega t)} \quad (26)$$

On free surfaces, the stresses are:

$\sigma_{zz} = \tau_{zx} = 0$ for $z = \pm\frac{h}{2} = \pm d$

Resulting in the homogeneous equation system of the symmetric wave of Eq. (25):

$$\begin{bmatrix} -2ikq_l \sin(q_l d) & (q_t^2 - k^2)\sin(q_t d) \\ -(q_t^2 - k^2)\cos(q_l d) & 2ikq_t \cos(q_t d) \end{bmatrix} \begin{bmatrix} A_2 \\ B_1 \end{bmatrix} = \begin{bmatrix} 0 \\ 0 \end{bmatrix} \quad (27)$$

And the anti-symmetric wave of Eq. (26):

$$\begin{bmatrix} 2ikq_l \cos(q_l d) & (q_t^2 - k^2)\cos(q_t d) \\ -(q_t^2 - k^2)\sin(q_l d) & -2ikq_t \sin(q_t d) \end{bmatrix} \begin{bmatrix} A_1 \\ B_2 \end{bmatrix} = \begin{bmatrix} 0 \\ 0 \end{bmatrix} \quad (28)$$

From the previous equations, Eq. (27) and (28), and by finding the determinants of them, the formulae of determinate the symmetric and anti-symmetric angular wavenumber k_{sym} and k_{anti} with given frequency has been created, which are denoted to *Lamb wave* equations, **Lammering, et al., 2017**, as:

$$\frac{\tan(q_t d)}{\tan(q_l d)} = \left[-\frac{4k^2 q_l q_t}{(k^2 - q_t^2)^2}\right]^{\pm 1} \quad (29)$$

The equation can be separated based on values of k_{sym} or k_{anti} as:

$$\frac{\tan(q_t d)}{\tan(q_l d)} = -\frac{4k^2 q_l q_t}{(k^2 - q_t^2)^2} \quad \text{for symmetric modes} \quad (30)$$

$$\frac{\tan(q_t d)}{\tan(q_l d)} = -\frac{(k^2 - q_t^2)^2}{4k^2 q_l q_t} \quad \text{for anti-symmetric modes} \quad (31)$$

This is the Lamb frequency equation for the propagation of symmetric anti-symmetric modes in a plate.

2.4 Dispersion Curves

The *phase velocity* c_p for a given angular excitation frequency ω and the associated angular wavenumber *k* have been calculated by the following relation **Wilcox, 1998**:

$$c_p = \frac{\omega}{k} \quad (32)$$

The phase velocity is the velocity at which the wave peaks of a continuous wave at a single frequency propagate, this leads to computing the dispersion curves. The phase velocity describes the velocity of wave peaks in a continuous single frequency wave, but a wave packet of finite

duration and therefore of finite bandwidth will propagate at a different velocity. This is called the *group velocity*, c_g , and is defined, **Wilcox, 1998** and **Lammering**, **et al., 2017**, as :

$$c_g = \frac{d\omega}{dk} \tag{33}$$

Rearranging Eq. (33) yields an expression for the group velocity in terms of the phase velocity and the angular frequency.

$$c_g = d\omega \left[d\left(\frac{\omega}{c_p}\right)\right]^{-1} = d\omega \left[\frac{d\omega}{c_p} - \omega \frac{dc_p}{c_p^2}\right]^{-1} = c_p^2 \left[c_p - \omega \frac{dc_p}{d\omega}\right]^{-1} \tag{34}$$

2.5 Lamb Waves in Plate of Multiple Layers

The Lamb waves dispersion equation has been given above were exact to the state of the flat isotropic plate. Elastic wave in multi-layer as polyester composite was of a large interest, and this subject was intensively studied in latest years along with the exponential increase of applications of advanced composite materials in the various manufacturing sector. The orthotropic natures of multi-layer structure introduce many singular phenomena as directionally depending on wave velocity and the difference in group and phase velocities.

Considering a plate comprised of homogeneous layers as shown in **Fig. 4**, the propagation of Lamb waves inside the plate includes not only scattering on the upper and lower surfaces but reflection and refraction between layers. Expanding Eq. (1) to an *N*-layered laminate, the displacement field, (*u, v and w*) within each layer must satisfy the Navier's displacement equations, and for the n^{th} layer, **Rose, 2014**:

$$\rho^n . \frac{\partial^2 u^n}{\partial_{t^2}} = (\lambda^n + \mu^n)\nabla(\nabla . u^n) + \mu^n(\nabla^2)u^n$$

$$\rho^n . \frac{\partial^2 v^n}{\partial_{t^2}} = (\lambda^n + \mu^n)\nabla(\nabla . v^n) + \mu^n(\nabla^2)v^n \tag{35}$$

$$\rho^n . \frac{\partial^2 w^n}{\partial_{t^2}} = (\lambda^n + \mu^n)\nabla(\nabla . w^n) + \mu^n(\nabla^2)w^n$$

The equation has been described by the superscript for each layer. Once more, the Helmholtz decomposition was the majority efficient method to analyze displacement fields and to obtain the stress, strain, and displacement in each odd layer. The propagation of Lamb waves in multi-layered structures cannot be described analytically and requires the numerical approach. The software which was used for most dispersion calculations uses the alternative *global matrix method*, as it is numerically more stable at high-frequency thickness values, **Demcenko,** and **Mazeika, 2010**.

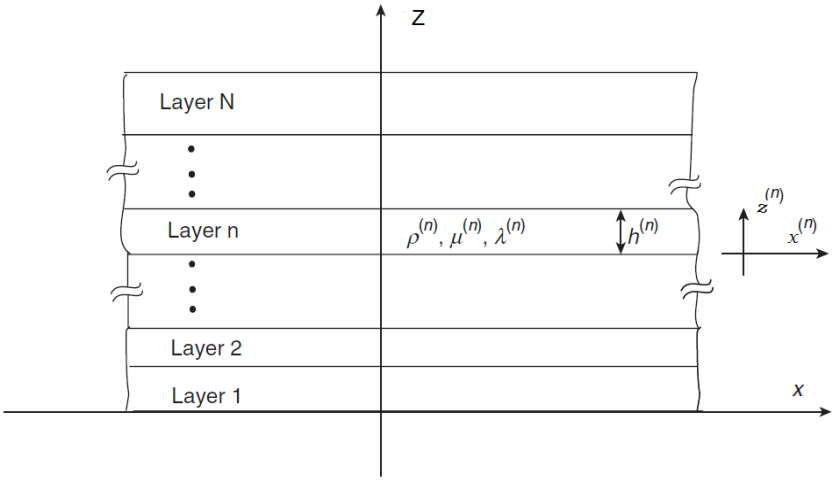

Figure 4. Geometry and the coordinate system of an *N*-layered plate, **Rose, 2014**.

3. LAMB WAVE SIMULATION USING ABAQUS SOFTWARE

In wave propagation analysis, the mesh and time increment size is highly dependent on the type of wave to be captured, the time increment size must be sufficient to capture the smallest period of interest and the element size should be small enough to capture wavelength but not smaller than one increment. Below are some important paragraphs which need clarification for the purpose of calculating the time increment size and element size and simulation of Lamb wave propagation using Abaqus software.

3.1 Elastic Wave Characteristics

Lamb wave propagation is dependent on the density and elastic modulus of a medium (Elastic wave propagation) with the longitudinal and transverse wave; the particle displacement is parallel and perpendicular to the direction of wave propagation respectively as shown in **Fig. 1**, Longitudinal and transverse wave speed depends on Young's and shear modulus, respectively.

$$c_t = \sqrt{\frac{G}{\rho}} \quad \text{(Transverse wave speed)} \tag{36}$$

$$c_l = \sqrt{\frac{\lambda+2\mu}{\rho}} \quad \text{(Longitudinal wave speed)} \tag{37}$$

Substitution the Eq. (2) into Eq. (37), the result is:

$$c_l = \sqrt{\frac{E(1-\upsilon)}{\rho(1+\upsilon)(1-2\upsilon)}} \tag{38}$$

3.2 Symmetric and Anti-Symmetric Mode

Typically, symmetric and anti-symmetric wave generated simultaneously for the general elastic medium is shown in **Fig. 5**. Since the existence of many modes in the response of high frequencies makes analysis difficult, isolating S_0 and A_0 from other modes (S_1, A_1, S_2……) is recommended to make analysis possible. From material properties dispersion curves of Lamb wave are calculated and from phase velocity dispersion curve the operating frequency selected, **Demcenko,** and **Mazeika, 2010** and **Maghsoodi, et al., 2014**, as shown in **Fig. 6**. The velocity of the Lamb wave mode is a function of (f·d) where f indicates the frequency and d indicates the plate thickness, expressed in MHz.mm.

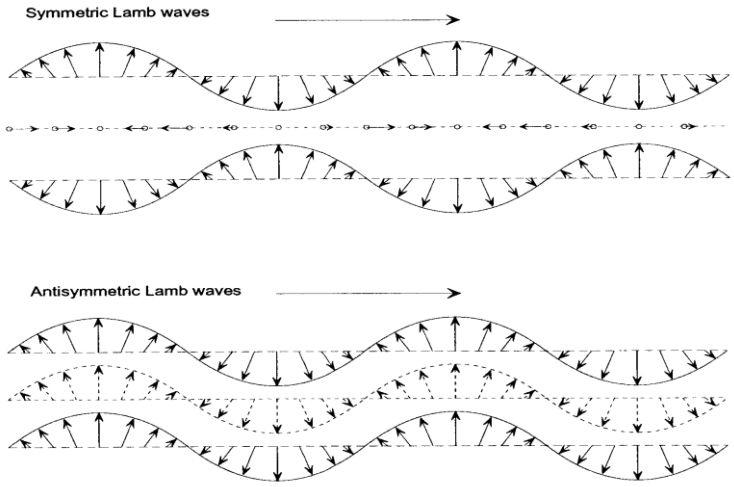

Figure 5. S_0 and A_0 to the multi-modal behavior of Lamb waves, **Orwat, 2001.**

In this research, (f·d) product is less than 0.5 MHz.mm. S_0 mode is the fastest wave as shown in dispersion curve in **Fig. 6**, is typically used as a signal for health monitoring.

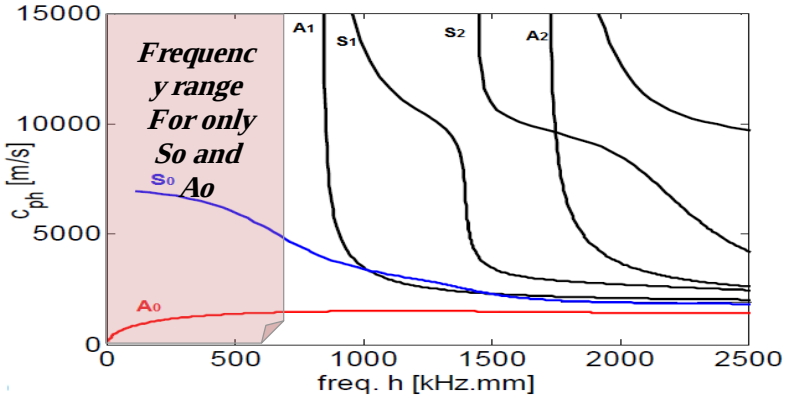

Figure 6. Lamb wave dispersion curves for a composite plate with cross-ply fiber [0^0/90^0].

3.3 Determining Element Edge Length

In order to capture propagation of Lamb wave, 10~20 elements per wavelength is a good mesh in order to show the form of wave properly. To choose proper element size first step is to calculate transverse wave speed. In this paper, the mechanical properties of the composite plate are shown in the **Table 1**.

$$C_t = \sqrt{\frac{G}{\rho}} = \sqrt{\frac{2.2189*10^9}{1613.9}} = 1172.54 \ \ m/s$$

The average thickness of the composite plate is 3.05 mm, f.d = 0.5 MHz.mm, therefore max frequency is 0.164 MHz and minimum smallest wavelength is calculated:

$$\lambda_{min} = \frac{C_T}{f_{max}} = \frac{1172.54}{0.164*10^6} = 7.15 * 10^{-3}\ m \qquad (min\ wavelength)$$

Therefore, typical (min ~ max) element size (L_{min}) would be ($3*10^{-4}$ ~ $7*10^{-4}$).

The element size also can be calculated with longitudinal wave speed ($C_l = 3153.2\ m/s$). The impulse of excitement signal has a wavelength of (~2×C_l×dt) where dt indicates the impulse time increment size, it is associated with operating frequency. 10 ~20 elements per wavelength is a good element size of mesh.

Table 1. The elastic constants of the woven composite specimen.

The property	The value
composite density (ρ_c) (kg/m^3)	1613.9
The fiber volume fraction (V_f)	28.638 %
The matrix volume fraction (V_m)	71.073 %
Elasticity modulus (E_{1w}=E_{2w}) (GPa)	15.1767
Elasticity modulus (E_{3w}) (GPa)	7.5376
Shear modulus (G_{12w}) (GPa)	2.3882
Shear modulus (G_{13w}) (GPa)	2.2189
Shear modulus (G_{23w}) (GPa)	2.2189
Poisson's ratio (υ_{12w})	0.1517
Poisson's ratio (υ_{13w})	0.498
Poisson's ratio (υ_{23w})	0.498

3.4 Determining Step Size

Adequate integration time step is important for accuracy, typically 20 points/cycle of the highest frequency results is reasonable, deciding time step needs two criteria; Courant, Fredrichs and Lewy criterion and Moser criterion, **Moser, et al., 1999**.

$$\Delta t < \frac{1}{20\, f_{max}} \quad , \quad \Delta t < \frac{L_{min}}{C_L}$$

Table 2 shows parameters along excitation frequency.

Table 2. The parameters along excitation frequency.

Excitation Freq.	100 kHz	10 kHz	1 kHz
Analysis frequency	1.00E+05 Hz	1.00E+04 Hz	1.00E+03 Hz
Min wavelength	1.15E-02 m	1.15E-01 m	1.15E+00 m
Min element size	1.15E-03 m	1.15E-02 m	1.15E-01 m
Δt [CFL] criterion	3.50E-07 sec	3.50E-06 sec	3.50E-05sec
Δt [M] criterion	5.00E-07 sec	5.00E-06 sec	5.00E-05 sec

The lower frequency which can travel longer needs high magnitude to avoid elastic wave attenuation. Therefore, frequency and magnitude of excitation signal need to be carefully considered. Excitation can be strain/displacement and stress/load. If PZTs were used for excitatory, the stress will be used as an excitation signal.

4. EXPERIMENTAL LAMB WAVE ANALYSIS

The damage detection using Lamb wave can be classified into two types, passive (pulse-echo) and active (pitch-catch) system as shown in **Fig. 7**. In the active system, Lamb wave is excited into structures using actuator and then sensed back by the sensor with damage information at the other side of the wave's paths. In a passive configuration, both source and sensor are located on the same side of the aim (object), and the sensor receives the echoed wave's signals from the aim. In this

experimental work, Lamb wave at ultrasonic frequencies passes through the thin elastic composite laminated plate to monitor plate integrity using pitch-catch configuration at different boundary conditions with and without a crack. Exciter and sensor include PZT wafer-type transducers.

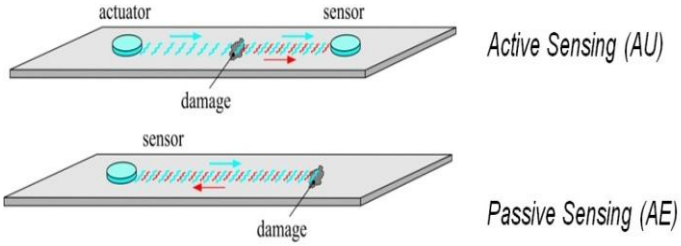

Figure 7. The damage detection in active and passive systems.

The testing model (composite laminated plate) with dimensions (285 mm long, 285 mm width and 3.05 mm thickness) was made up polyester reinforced by five-layer woven fiberglass $[0^0/90^0]_5$ by using hand lay-up process. Samples are made from manufactured composite laminated plate and tested to evaluate mechanical properties.

4.1 Experimental Setup

The experimental set-up was established to obtain all necessary damage detection testing results. This set-up makes use of National Instruments LabVIEW software. A program was created to control the waveform type, frequency, and amplitude. The diagram view of the experimental setup as illustrated in **Fig. 8**. A function analog input (NI 9215), function analog output (NI 9263) and data acquisition (NI cDAQ-9178) selected from *National Instruments (NI)* is used for data.

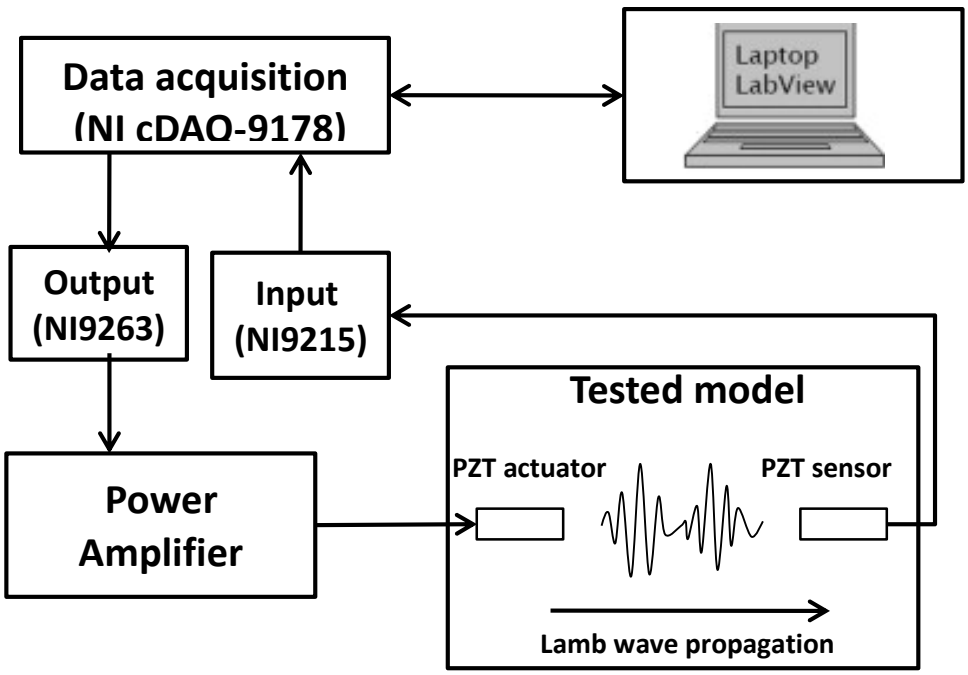

Figure 8. Schematic view of the experimental setup.

A piezoelectric actuator excite the specimen by the lamb wave signals which was created by computer control using LabVIEW software, the output signals from (PC Laptop) was sent to data acquisitions (NI cDAQ-9178) and analog output DAQ (NI 9263), then the lamb wave signals with ± 5V was sent to Piezo Driver type TREK 2205, then the amplifier sent it with ± (50-60) V to the PZT actuator to excite the plate by this signal.

The lamb wave propagates through the plate and is captured by the PZT sensor from the end of the wave propagation. The PZT sensor data is sent to (NI cDAQ-9178) through analog input DAQ NI 9215 which converts the signal from Analog to Digital, then sensor data appears in LabVIEW software on PC Laptop. The input signal to the DAQ was limited by ± 10 V. Bayonet Neill–Concealment (BNC) cable was used for connecting between the devices and transmission of the signal through it. The oscilloscope device and voltage monitor (AVOmeter) were used to check the input lamb wave signal and voltage to the PZT actuator, the experimental set-up with the laboratory devices are shown in **Fig. 9**.

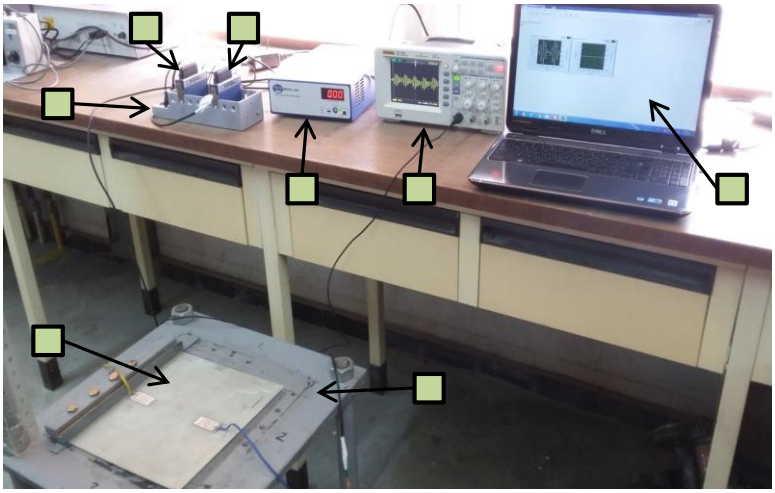

Figure 9. The experimental set-up. (1)- LabVIEW. (2)- Digital Oscilloscope. (3)- Power Amplifier. (4)- NI cDAQ-9178. (5) - DAQ (NI 9263). (6) - DAQ (NI 9215). (7) - Smart Plate. (8)- Rig.

4.2 Lamb Wave Excitation

In the experimental study and numerical simulation, the PZT actuator was excited by lamb wave signal, it was driven by a windowed sinusoid of the form:

$$V_{(t)} = \begin{cases} V_0 \sin(\omega t) \cdot \left(\sin\left(\frac{\omega t}{10}\right)\right)^2 & t < \frac{10\pi}{\omega} \\ 0 & otherwise \end{cases} \quad (39)$$

Where, V_0 = 5 volt and ω represents the angular frequency. The frequency (f) in the experimental test was varied from 10 to 50 kHz. The excitation was generated by computer control using LabVIEW. **Fig. 10** illustrates the waveform of this excitation.

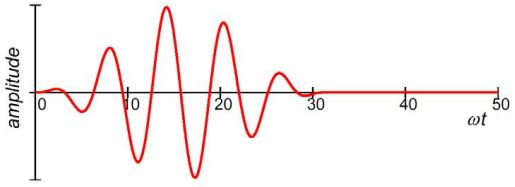

Figure 10. Excitation waveform.

Creation an analog signal with Lamb waveform is illustrated in **Fig. 11** and **Fig. 12** shows the response signal of the composite plate before and after filtration (Bessel filter).

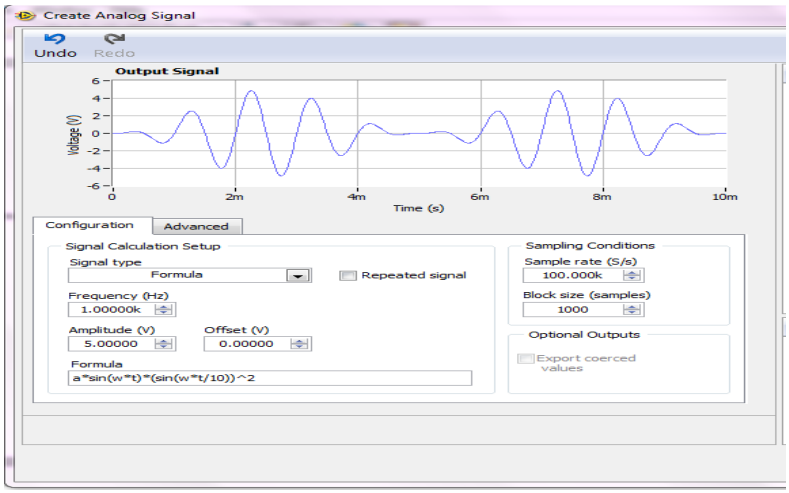

Figure 11. Creating Lamb wave signal at 1 kHz and 5 volts.

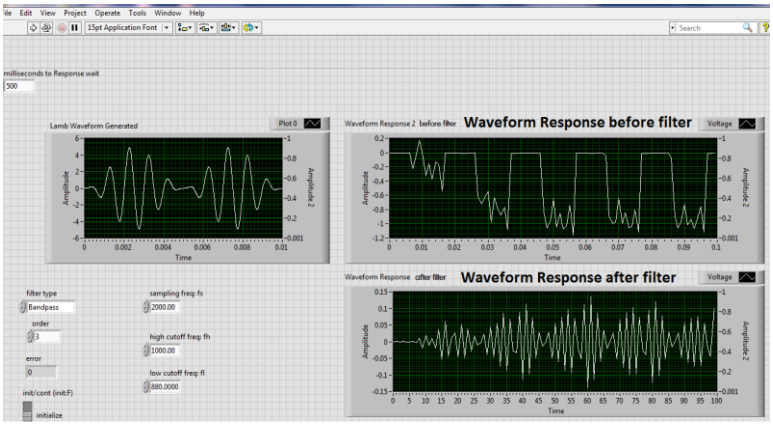

Figure 12. Response signal for (CFFF) intact plate before and after filtration.

5. LAMB WAVE PROPAGATION RESULTS

This section presents the results of numerical simulation and experimental procedures for Lamb wave propagation in a plate with and without a crack.

5.1 Numerical Simulation Results

The first set of results obtained from the FEM model created in Abaqus software is shown in **Fig. 13**. This figure illustrates the simulation of the Lamb wave's behavior and analyzes its travel across the composite laminate plate with and without crack, at (0~350) microsecond intervals and (100 kHz) with (CCCC) boundary condition. The results of these analyses were taken from the movie files which moved the vertical displacement of the nodes over time as the waves propagated from the loaded nodes. The FEM results did not show much of a change between the intact plate and defect plate for the time of travel, however, there was a notably reflected wave traveling from the crack region after the wave passed over it. The results prefer Black-White spectrum for wave propagation because easy to see its pattern.

The second set of results is Time-trace of the voltage signal from the PZT sensor; it is a convenient way to show differences between recorded signals, it is amplitude representation with (x, y) direction. **Fig. 14** illustrates the comparison of numerical results between the signals for the intact plate and defect plate with crack dimensions (20 mm long, 0.4 mm width and 3.05 mm thickness), the excitation signals with (5V) amplitude and (1 kHz) frequency with various boundary conditions. The response signals in two states show a clear change in amplitude and phase at S_0 mode. Although there is a significant change caused by damage in signals amplitude, this study focuses only on delaying the time of the signal because the time of Lamb wave propagation can be measured more minutely in the experimental test, while the amplitude of the signals may vary due to the different bonding conditions of the PZT sensors.

From the results, it can be noticed that for every wave path that passes the crack region, the corresponding wave package will be delayed in phase because the S_0 wave is very dispersive at low-frequency range, and slight loss of stiffness in the crack region leads to a marked change in phase velocity. Finally, the oscillations in the curve progression are a result of the interference of wave groups.

5.2 Experimental Results

The magnitude of the diagnostic Lamb wave signal and response signal of the composite laminated plate increases proportionately with an increase in the excitation voltage. Usually, activation of a PZT actuator at 1~10 V can create a response signal of 2~25 mV, with accompanying noise at the level of 0.2~5 mV, **Zhongqing,** and **Lin, 2009**. **Fig. 15** illustrates the result of experimental verification for the response signal of the specimen when the excitation voltage was (1V). In this experimental work, the Lamb wave signals were excited with (5V) amplitude and various value of frequency.

In this experimental work, the form of damaged plates has been investigated as a simple plate. The damage was a crack created in the composite laminated plate by hand using electric cutting tool with dimensions (20 mm length and 0.4 mm width) through whole plate thickness in the middle of the plate. The cutting tool was passed in the crack on the other side of the plate to adjust the edge and depth of the crack.

The experimental results for time-trace of the voltage signal from the PZT sensor shown in **Fig. 16** and **Fig. 17**, it illustrates the comparison between the intact and defect plate signals with (CCCC) and (CFFF) boundary condition, respectively. The comparison shows a clear difference between the two signals due to the presence of the crack, the reason was explained in the paragraph above.

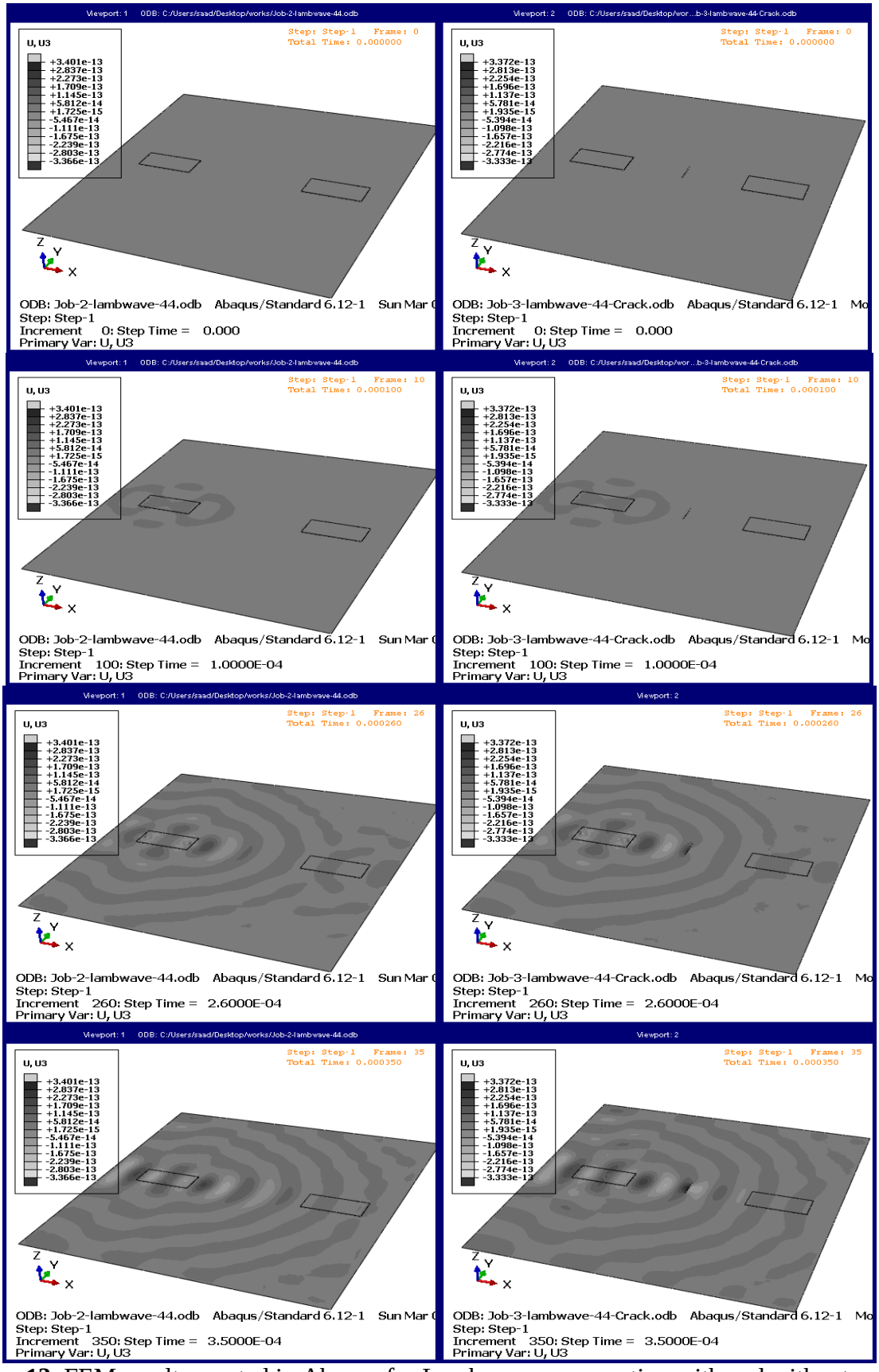

Figure 13. FEM results created in Abaqus for Lamb wave propagation with and without a crack at (0~350) microsecond intervals, 100 kHz and (CCCC) BC.

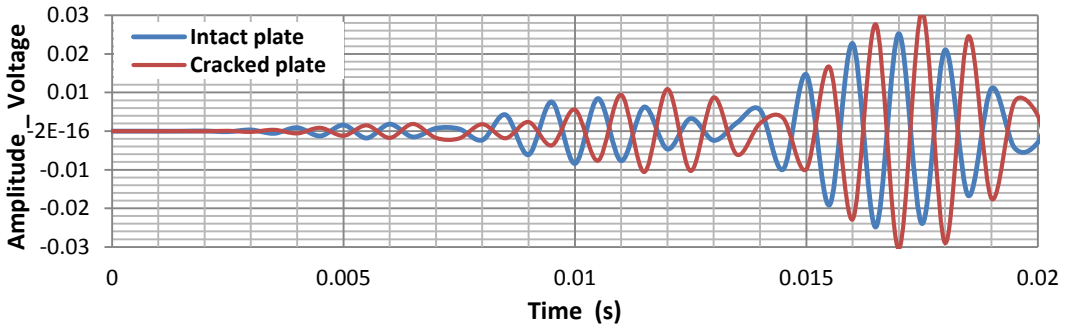

(CCCC)

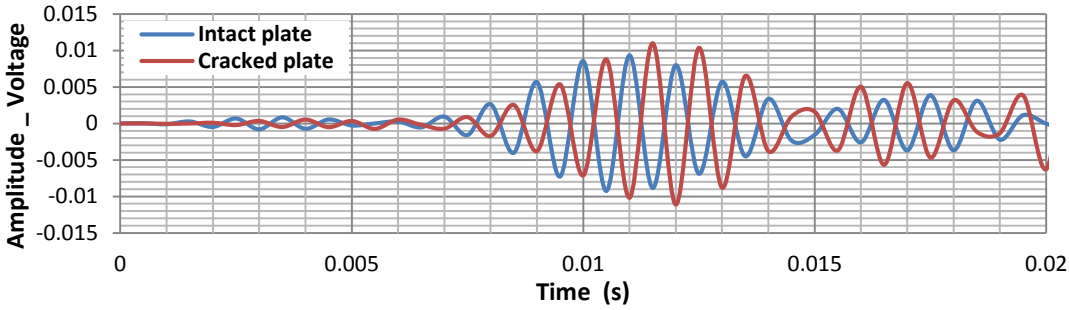

(CFFF)

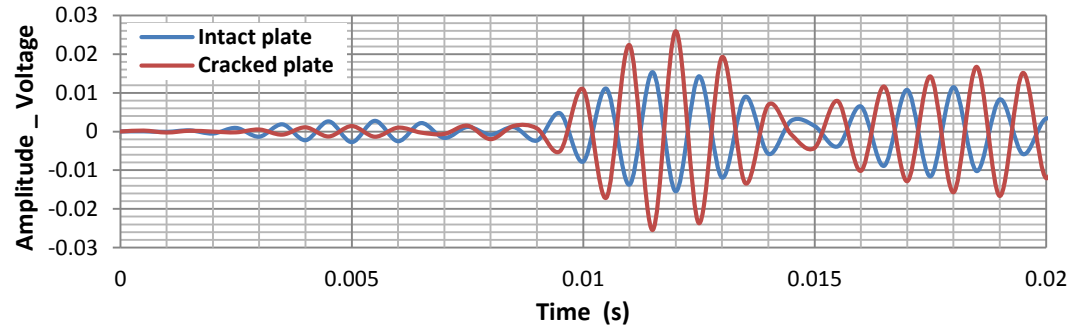

(SSSS)

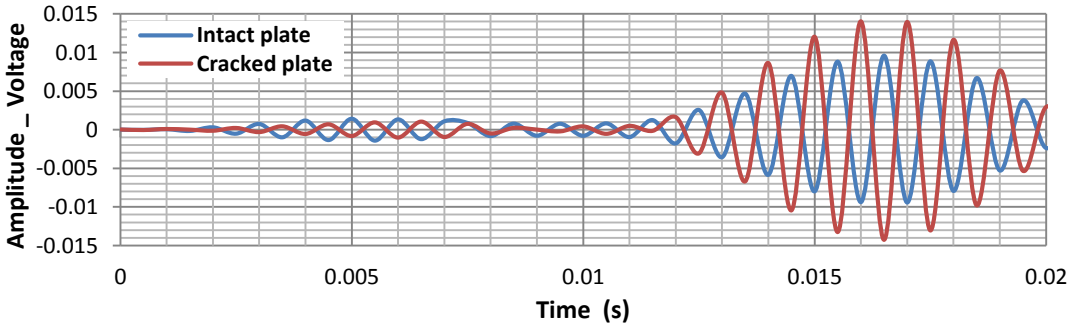

(SFSF)

Figure 14. The numerical results for intact and defect plate signals with crack dimensions (20x0.4x3.05) mm, (1 kHz) frequency, and various boundary conditions.

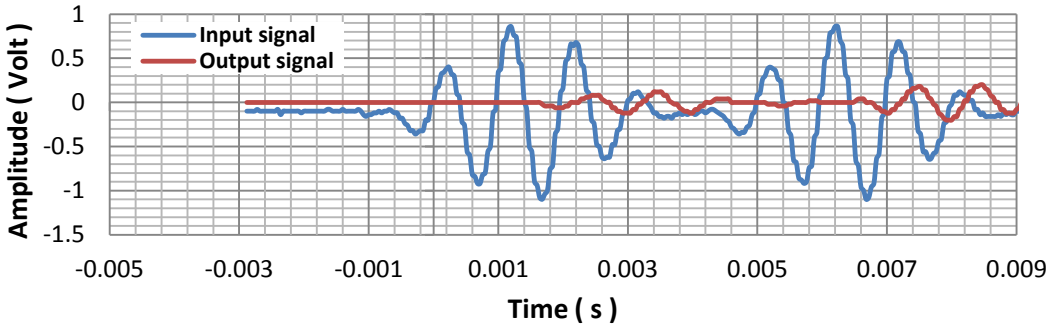

Figure 15. The result of experimentally verification for the response signal of the composite laminated plate**,** excitation voltage was (1V).

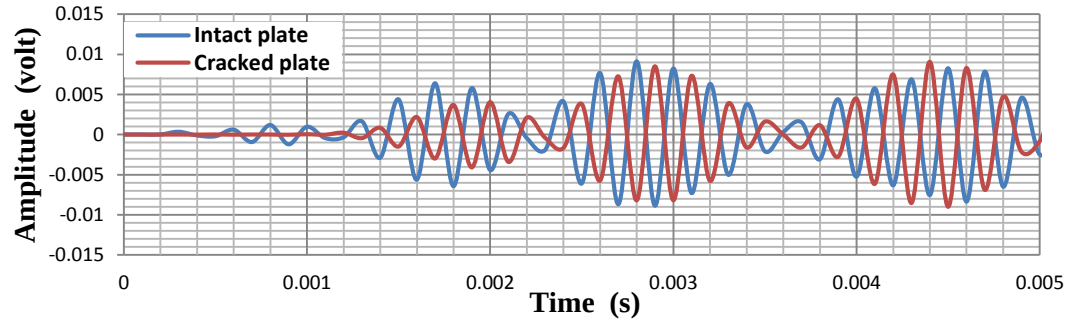

10 kHz

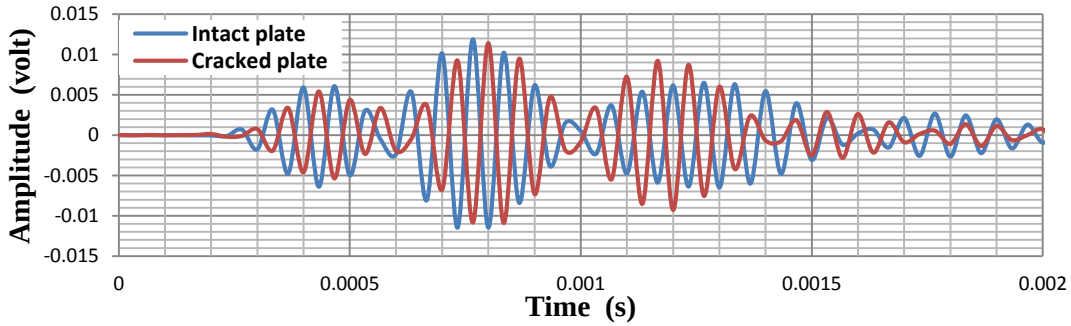

30 kHz

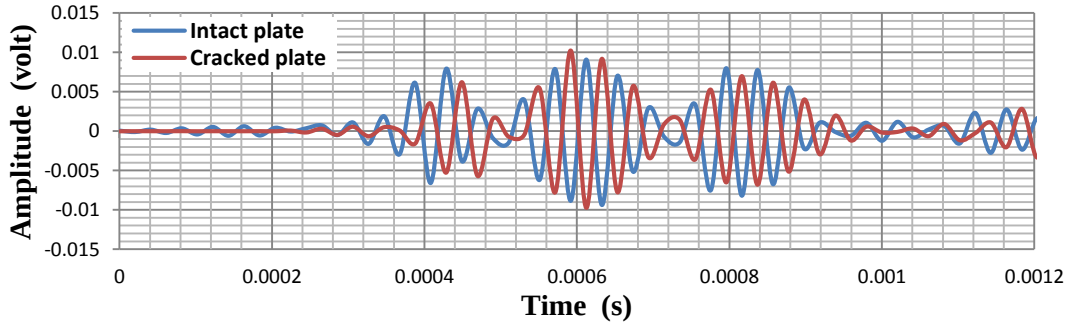

50 kHz

Figure 16. Experimental results for intact and defect plate signals with crack dimensions (20x0.4x3.05) mm, (CCCC) BC and various value of frequency.

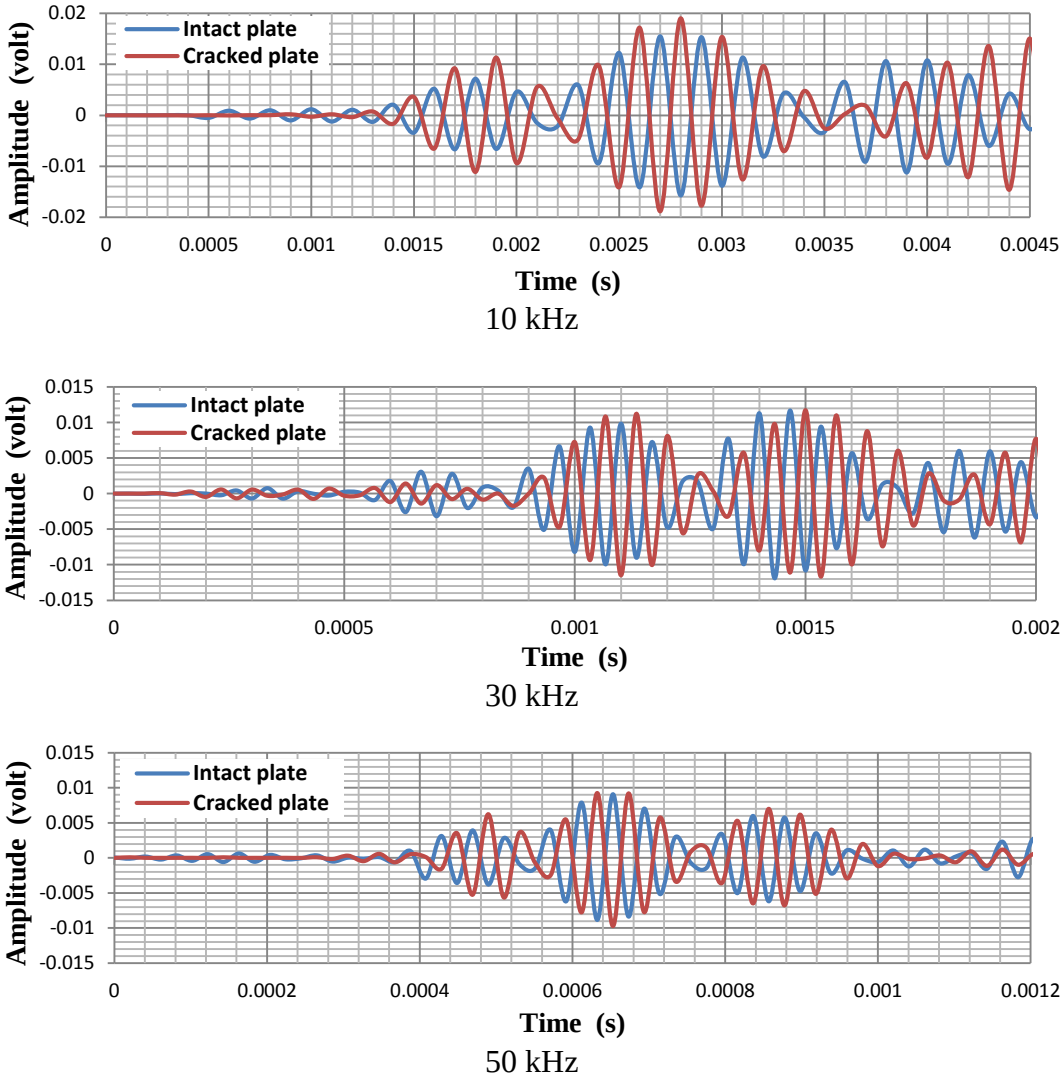

Figure 17. Experimental results for intact and defect plate signals with crack dimensions (20x0.4x3.05) mm, (CFFF) BC and various value of frequency.

5.3 Comparison between Numerical and Experimental Signal Results

During numerical and experimental testing, it was noticed that choosing the location of the sensor has a great effect on the possibility of a detection of crack. Therefore, to increase the probability of defect detection many testing measurements should be made at different sensor positions. In this numerical and experimental results one sensor was used and the crack wa created in the middle of the distance between the sensor and actuator. **Fig. 18** illustrates the comparison between numerical and experimental results for the amplitude and travel times of response signal in the plate with and without crack with (CCCC) boundary condition. Good agreement was found between the signals at (1.3 ms) of data, the deviations between the results resulting from some possible measurement errors such as; noise effects, non-uniformity in the properties of the specimen, nonuniform surface finishing, and variations in thickness voids. From **Fig. 18 a**, the average amplitude is (0.0124 V) and (0.0154 V) for numerical and experimental signal respectively, and the error ratio is (19.48 %) and From **Fig. 18 b**, the average amplitude is (0.0151 V) and (0.0136 V) for numerical and experimental signal respectively, and the error ratio is (11.03%). This proves that the transmitter-receiver damage detection using Lamb wave is viable and implementable.

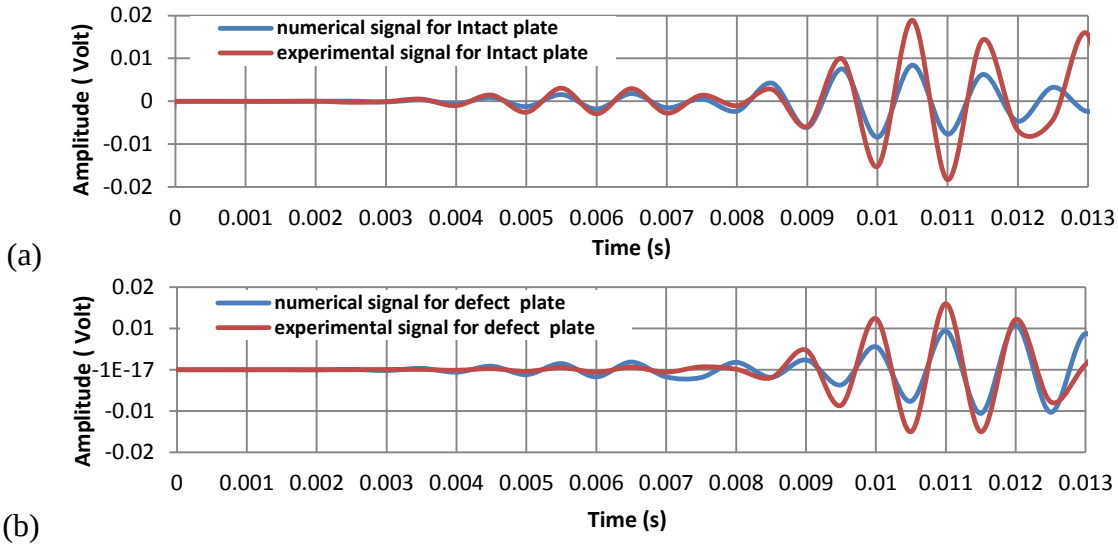

Figure 18. Comparison between numerical and experimental results (amplitude and travel times) of the response signal at (1.3 ms) of data :(a) intact plate, (b) defect plate with crack with (CCCC).

6. CONCLUSIONS

1. The study in this paper was focused only on the crack detection in the multi-layer composite plate $[0^0/90^0]_5$. However, other types of damage can be detected with the same analysis and experiments in composite or metal materials. This is possible in future investigations.
2. The operation of a PZT has been analyzed using a combination of finite element simulation and experiments to excite and detect the Lamb waves which were used to detect damage.
3. For every wave path that passes through the crack region, the corresponding wave package will be delayed in phase because the S_0 wave is very dispersive at low-frequency range, and slight loss of stiffness in the crack region leads to a marked change in phase velocity.
4. The results show that Lamb wave propagation is a good technique for the identification of damage in the composite laminated plate with high accuracy; also it is sensitive to small damage.
5. Through experimental tests and numerical simulations in this study, it was found that the PZT wafer transducer can be used for the eclectic irritation of the S_0 mode that use to damage detection.
6. As a future works in the field of composite laminated structures, can be taken into consideration studying the identification the size and location of damage in composite structures using Lamb waves with multiple actuators and sensors, also, more work latent in the future for different types of built-up structures, other than those tested during the current search, as joined sections and sandwich structures, etc.

REFERENCES

- Graff, K. F., 1975, *Wave Motion in Elastic Solids*, Oxford University Press.
- Rose, J. L., 2014, *Ultrasonic Waves in Solid Media*, Cambridge University Press, ISBN 978-1-107-04895-9.
- Kessler, S.S., Spearing S.M. and Soutis, C., 2003, *Structural health monitoring of built-up composite structures using Lamb wave methods*, submitted to Journal of Intelligent Material Systems and Structures.

- Giurgiutiu, V., and Zagrai, A.N., 2000, *Characterization of piezoelectric wafer active sensors, Journal of Intelligent Material Systems and Structures*, Vol. 11, 959-975.
- Giurgiutiu, V., 2002 *Lamb Wave Generation with Piezoelectric Wafer Active Sensors for Structural Health Monitoring,* SPIE Smart Structures Conference, San Diego, paper 5056-17.
- Nieuwenhuis, J. H., Neumann, J., Greve, D. W., and Oppenheim, I. J., 2004 *Generation and detection of guided waves using PZT wafer transducers*, submitted to IEEE Trans. Ultrasonics, Ferroelectrics, and Frequency Control.
- Paul D. Wilcox, 1998, *Lamb wave inspection of large structures using permanently attached transducers,* Department of Mechanical Engineering, Imperial College of Science, Technology and Medicine, London SW7 2BX.
- A. M. Howatson, P. G. Lund, J. D. Todd, 1972, *Engineering tables and data"* Department of Engineering Science, University of Oxford, Springer Netherland.
- R. Lammering, U. Gabbert, M. Sinapius, T. Schuster, P. Wierach, AG 2017. *Lamb-Wave Based Structural Health Monitoring in Polymer Composites*" Research Topics in Aerospace, Springer International Publishing.
- A. Demcenko and L. Mazeika, 2010, *Calculation of lamb waves dispersion curves in multi-layered planar structures*, Journal of Sound and Vibration, vol. 329, no. 9, pp. 1435–1449.
- A. Maghsoodi, A. Ohadi, M. Sadighi, 2014, *Calculation of Wave Dispersion Curves in Multilayered Composite-Metal Plates,* Hindawi Publishing Corporation, Shock and Vibration, Vol., Article ID 410514, 6 pages.
- Friedrich Moser, Laurence J. Jacobs, Jianmin Qu, 1999, *Modeling elastic wave propagation in waveguides with the finite element method*, NDT & E International, 32(4), 225-234. Elsevier Science Ltd.
- Zhongqing Su and Lin Ye, 2009, *Identification of Damage Using Lamb Waves*, LNACM 48, pp. 1–14, Springerlink.com © Springer-Verlag Berlin Heidelberg.
- Mark E. Orwat, 2001, *Experimental Investigation of Lamb Waves in Transversely Isotropic Composite Plates"* Master of Science in Civil and Environmental Engineering, Massachusetts Institute of Technology.

NOMENCLATURE

A_0 = initial Anti-symmetry mode
c_l = longitudinal wave velocity, m/s.
c_t = transverse wave velocity, m/s.
E = elastic modulus, GPa.
f = centrifugal force per unit volume, N/m^3.
G = shear modulus, GPa.
h = total thickness of plate, m.
k = wavenumber.
S_0= initial symmetry mode
t = time, sec.
u = displacement in x directions, m.
v = displacement in y directions, m.
V_f = fiber volume fraction.
V_m = matrix volume fraction.
w = displacement in z directions, m.
ρ = density, kg/m^3.
σ = normal stresse, N/m^2.
τ = shear stresse, N/m^2.
ω = angular natural frequency, rad/sec.
υ = Poisson ratio.
λ_{wave} = wavelength, m.
λ, μ = Lame's stiffness constant
$\emptyset$,$\vec{\psi}$ = scalar and vector field.